Sensors and Actuators B 244 (2017) 684–692

Contents lists available at ScienceDirect

Sensors and Actuators B: Chemical

journal homepage: www.elsevier.com/locate/snb

# Solvothermal synthesis of CoS/reduced porous graphene oxide nanocomposite for selective colorimetric detection of Hg(II) ion in aqueous medium

Priyakshree Borthakur[a,b], Gitashree Darabdhara[a,b], Manash R. Das[a,b,*], Rabah Boukherroub[c], Sabine Szunerits[c]

[a] Advanced Materials Group, Materials Sciences and Technology Division, CSIR-North East Institute of Science and Technology, Jorhat 785006, Assam, India
[b] Academy of Scientific and Innovative Research, CSIR-NEIST Campus, India
[c] Univ. Lille1, CNRS, Centrale Lille, ISEN, Univ. Valenciennes, UMR 8520 – IEMN, F-59000 Lille, France

ARTICLE INFO

*Article history:*
Received 28 October 2016
Received in revised form
23 December 2016
Accepted 31 December 2016
Available online 2 January 2017

*Keywords:*
Reduced porous graphene oxide
Cobalt sulphide nanoparticles
Peroxidase
Heavy metal ions
Sensing

ABSTRACT

Metal sulphide nanoparticles (NPs) have great potential applications in environmental remediation as they can oxidize peroxidase substrates like 3,3′,5,5′-tetramethylbenzidine (TMB) due to the production of hydroxide radicals ($OH^{\bullet}$) via the Fenton reaction in presence of $H_2O_2$. Their good binding affinity toward heavy metal ions through their S-containing sites, causes the blockage of the active sites of the catalyst and inhibits the oxidation process of peroxidase substrate. This property can be used for the sensing of heavy metal ions. Herein, a cobalt sulphide (CoS) decorated porous reduced graphene oxide (p-rGO) nanocomposite is proposed as a novel matrix for heavy metal ions detection in aqueous medium. The nanocomposite was fabricated by adopting a simple and easy solvothermal approach. After determination of the kinetics of the as-synthesized nanocomposite for the oxidation of TMB in presence of $H_2O_2$, the matrix was further used for the colorimetric detection of heavy metal (Hg, Pb, Cd) ions in aqueous medium. Depending on the metal ion, a detection limit of 14.23 nM for Hg(II) could be reached. Furthermore, the synthesized nanocomposite was successfully utilized for the detection of heavy metal ions present in real samples.



## 1. Introduction

Heavy metal ions are major hazardous environmental pollutants which can affect negatively the environment as well as public health [1]. Due to high solubility in aqueous solutions, they can undergo excessive accumulation in the aquatic ecosystem [2]. In case of carcinogenic mercury ions ($Hg^{2+}$) severe damages to kidney, heart, respiratory and nervous systems in humans and animals are reported [3–5]; high levels of lead ($Pb^{2+}$) ions are affecting the rate of human growth [6], while cadmium ions ($Cd^{2+}$) are extensively used in several industries and agriculture and can affect the human lung, kidney, bone, liver, immune and cardiovascular systems. $Cd^{2+}$ ion is also dangerous to the living organisms due to its longer accumulation time in the environment as well as its long half-life period of about 30 years [7]. Thus the development of a simple, facile, cost effective, selective, sensitive and reliable method for the identification of heavy metal ions in environmental samples has become a great challenge and a focus of many researchers.

Analytical approaches such as atomic absorption spectroscopy (AAS) [8], atomic fluorescence spectroscopy [9], liquid chromatography [10], inductively coupled plasma mass spectrometry (ICP-MS) [11,12], inductively coupled plasma-atomic emission spectrometry [13], electrochemical [14] as well as high-performance liquid chromatography (HPLC) [15] are mainly exploited currently. These analytical techniques require however expensive instruments and complicated pre-treatment procedures thus limiting their practical applications.

The use of nanomaterials in colorimetric detection of heavy metal ions is considered as a simple and an easy to operate analytical approach. In recent years, metal nanoparticles based nanocomposite materials are successfully utilized as colorimetric probes for the detection of heavy metal ions based on the colour change of the 3,3′,5,5′-tetramethylbenzidine (TMB)-$H_2O_2$ system [16–19]. Tan et al. used Au nanoparticles supported on hollow

* Corresponding author at. Advanced Materials Group, Materials Sciences and Technology Division, CSIR–North East Institute of Science and Technology, Jorhat 785006, Assam, India.
*E-mail addresses:* mnshrdas@yahoo.com, mrdas@neist.res.in (M.R. Das).

http://dx.doi.org/10.1016/j.snb.2016.12.148
0925-4005/

fibre liquid membrane for the colorimetric detection of $Hg^{2+}$ ions [20]. Chen and co-workers developed graphene oxide-gold nanohybrids and utilized them for the colorimetric detection of $Hg^{2+}$ and $Pb^{2+}$ in the presence of single-stranded DNA (ssDNA) [21]. The presence of sulphur containing functional groups in the nanocomposite materials proved to be a good strategy to integrate metal ions binding sites based on the stronger affinity of metal ions and S-containing ligands. It has been shown lately that, while metal sulphide nanoparticles catalyse the oxidation of peroxidase substances in presence of $H_2O_2$, the strong binding affinity toward heavy metal ions causes the blockage of the active sites of the catalyst and results in the inhibition of the oxidation process [22]. This assay was used for the colorimetric detection of Hg(II) ions [22].

In this work we investigate the potential of cobalt sulphide (CoS) nanostructures embedded on reduced porous graphene oxide (p-rGO) as a novel metal ion sensing platform, based on the inhibition of peroxidase-like activity. Most of the chalcogenide materials supported on graphene sheets have shown peroxidase like activity [23–25]. The presence of graphene sheets in metal sulphide/graphene nanocomposite materials enhances the peroxidase-like activity due to their synergistic effect. We demonstrate herewith that the synthesized CoS-p-rGO nanocomposite increases the peroxidase like activity when compared to other graphene based catalysts because of the high surface area and large pore size of the nanocomposite. The interest of the integration of CoS onto p-rGO is that CoS is cheap, highly abundant and biocompatible. Co(II) ions can in addition decompose peroxide substrates to hydroxyl radicals [26]. Herein CoS /p-rGO nanocomposite was synthesized by a simple solvothermal method and its peroxidase like activity toward colorimetric detection of heavy metal ions like Hg (II) ions is demonstrated.

## 2. Materials and methods

### 2.1. Materials

Cobalt(II) nitrate hexahydrate (98%, Sigma-Aldrich, India), thiourea (99%, Merck, India), graphite powder (<20 μm, Sigma-Aldrich), sulfuric acid (AR grade, Qualigens, India), potassium permanganate (>99%, E-Merck, India), hydrochloric acid (AR grade, Qualigens, India), hydrogen peroxide (30%, Qualigens, India), sodium hydroxide (99%, Qualigens, India), polyvinylpyrrolidone (M.W. 10,000, Alfa Aesar, India), 3,3′,5,5′-tetramethylbenzidine (TMB, >99%, Sigma-Aldrich, USA), mercuric chloride (99.5%, Qualigens, India), lead (II) acetate (99.5%, Sd fine Chem.), cadmium chloride (Loba Chemie, India), mercury (I) nitrate dihydrate ( > 97.0%, Sigma Aldrich, India), phenol (Alfa Aesar, India), sodium humate (Sigma Aldrich, India) were used as received. Chlorophyll green algae, containing both chlorophyll a and b, was collected from the pond of CSIR-NEIST campus, Jorhat.

### 2.2. Synthesis of porous graphene oxide (p-GO)

Graphite oxide was synthesized adopting the modified Hummers and Offemann's method [27]. The synthesized graphite oxide was dispersed at a concentration of 1.5 mg/mL in 500 mL DI water by ultrasonication for 1 h to obtain a homogeneous suspension of graphene oxide (GO). Then 0.5 g of NaOH was added to the suspension and the mixture was heated at 120 °C under magnetic stirring for 90 min. The base treated GO was separated by centrifugation and again dispersed in 500 mL DI water by ultrasonication. The mixture was then heated for 90 min at 120 °C after the addition of 20 mL of 37% HCl solution. The final product was filtered and washed with DI water and acetone. The synthesized p-GO was dried in a desiccator under vacuum [28].

### 2.3. Synthesis of CoS-p-rGO

To synthesize CoS-p-rGO nanocomposite, 16 mg of polyvinylpyrrolidone (PVP) was added to 20 mL of 0.1 mg/mL of p-GO suspension in 1:1 (v:v) ratio of ethylene glycol and DMF and allowed to stir for 30 min. 0.025 mmol of $Co(NO_3)_2{\cdot}6H_2O$ was added to the suspension followed by 20 mL of 0.075 mM thiourea solution. The mixture was then stirred for 30 min at room temperature for homogeneous distribution and then transferred into a Teflon lined autoclave and kept at 180 °C for 6 h. After cooling to room temperature the product was filtered, washed with DI water and ethanol and dried in an air oven at 60 °C for 4 h.

### 2.4. Characterization

The crystal structure of the synthesized nanocomposite was investigated by powder X-ray diffraction (XRD) analysis. XRD patterns were recorded using Rigaku X-ray diffractometer (Model: ULTIMA IV, Rigaku, Japan) with a scanning rate of 3° $min^{-1}$ and 2θ value ranging from 5 to 100° using Cu Kα (λ = 1.54056 A) as the X-ray source and operates at a generator voltage of 40 kV and current 40 mA, respectively. Fourier transform infrared (FT-IR) spectra were recorded using IR Affinity, Shimadzu, Japan FT-IR spectrophotometer equipped with a Shimadzu DRS-8000 DRIFT accessory and IR solution software with 4 $cm^{-1}$ spectral resolution.

The surface morphology of p-GO sheets and the nanocomposite were analysed by field emission scanning electron microscopy (FESEM) using ZEISS Gemini scanning electron microscope (Germany) operated at an accelerating voltage of 9–7 kV. The morphology and crystal structure of the materials were examined by transmission electron microscope (TEM) and high-resolution TEM (HRTEM) using a JEOL JEM 2100, transmission electron microscope (Japan) operated at an accelerating voltage of 200 kV. For analysis, dispersed colloidal solutions of nanocomposite were prepared and dropped onto standard carbon-coated copper grids and then air dried at room temperature.

X-ray photoelectron spectroscopy (XPS) of the synthesized nanocomposite was recorded using ESCALAB 220 XL spectrometer from Vacuum Generators featuring a monochromatic Al Kα X-ray source (1486.6 eV) and a spherical energy analyser operated in the constant analyser energy (CAE) mode (for survey spectra CAE = 100 eV and for high-resolution spectra CAE = 40 eV), using the electromagnetic lens mode. The angle between the incident X-rays and the analyser is 58° and the detection angle of the photoelectrons was 30°.

The specific surface area of the synthesized CoS-p-rGO nanocomposite was examined by nitrogen gas adsorption study at 77 K by using an Autosorb-iQ Station 1 (Quantachrome, USA) and applying Brunauer–Emmett–Teller (BET) calculations. Before performing the experiments, the samples were degassed at 200 °C for 3 h.

The catalytic oxidation of TMB and colorimetric detection of heavy metal ions were monitored using a UV–vis spectrophotometer (MS-11-UV-1800, Shimadzu, Japan).

### 2.5. Determination of peroxidase-like activity of CoS-p-rGO

0.5 mM TMB and 50 μL of 30% $H_2O_2$ were added into 2.5 mL sodium acetate buffer (pH 3) and the reaction mixture was incubated at 45 °C for 30 min, followed by investigation of the formation of oxidation product of TMB using UV–vis spectrophotometer at 652 nm. The effect of CoS-p-rGO concentration on the catalytic reaction was investigated over the range of 3–7 mg/L. The effect of pH on the catalytic reaction was evaluated by carrying out the reaction at varying pH from 2 to 7. The temperature effects were studied by varying the temperature from 25 to 55 °C.

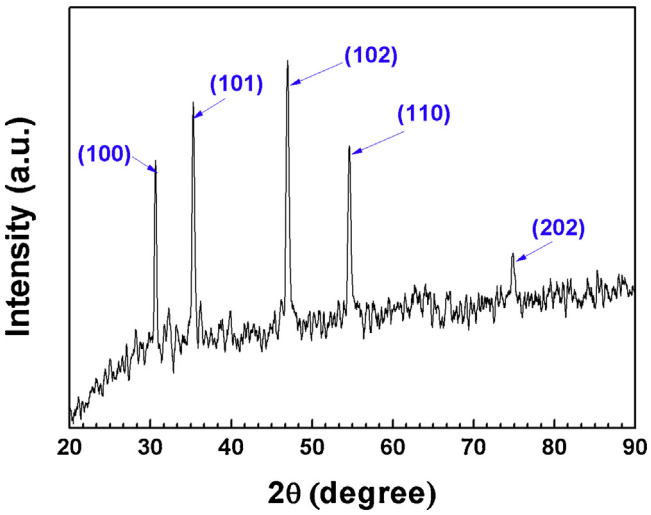


**Fig 1.** XRD pattern of CoS-p-rGO nanocomposite.

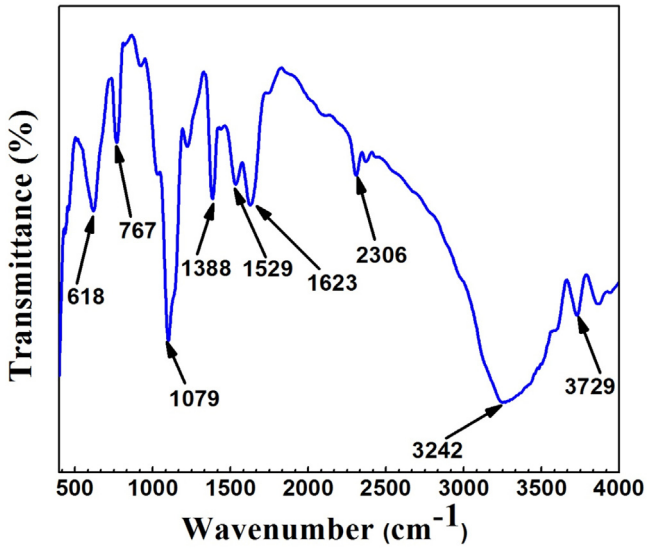


**Fig. 2.** FTIR spectrum of CoS-p-rGO nanocomposite.

Typical Michaelis-Menten curves for CoS-p-rGO nanocomposite were obtained by varying the concentrations of both TMB and $H_2O_2$ over a certain concentration range. The affinity of the enzyme towards the substrate was determined from the Lineweaver-Burk double reciprocal plot. The equation of the Lineweaver-Burk plot is represented as:

$$1/V = K_m/V_m[S] + 1/V_m$$

where $V$ is the initial rate of the reaction, $V_m$ is the maximal rate of the reaction and [$S$] is the substrate concentration.

### 2.6. Detection of heavy metal (Hg(II)) ions in aqueous medium

For the detection of heavy metal ions like Hg(II), different concentrations of $HgCl_2$ were added to a mixture containing 0.5 mM TMB, acetate buffer (0.2 M, pH 3, 2.5 mL), 7 mg/L catalyst and 50 μL $H_2O_2$. The volume of the mixture was adjusted to 5 mL by adding acetate buffer. After that the mixture was incubated at 45 °C for 30 min. The UV–vis spectra of the mixture were monitored at the wavelength of 652 nm.

### 2.7. Detection of Hg(II) ions in environmental samples

The practical applicability of the suggested method was investigated by spiking different concentrations of Hg(II) ion into various environmental water samples (i.e tap, pond, tube well and river water). The tap water samples were collected from CSIR-NEIST, Jorhat. The pond and tube well water were collected from local area of Jorhat city, Assam, India and river water samples were collected from the Brahmaputra River (Jorhat, Assam, India). The collected water samples were filtered through a filter membrane with pore size 0.22 μm and standard solutions of Hg(II) ions (10, 30, 100 nM) were added separately and analysed by the same procedure as discussed above.

## 3. Results and discussion

### 3.1. Characterization of CoS-p-rGO nanocomposite

The crystalline structure of the synthesized nanocomposite was monitored by powder XRD analysis. Fig. 1 shows the XRD pattern of the synthesized CoS-p-rGO nanocomposite material. The major diffraction peaks (100), (101), (102), (110) and (202) at corresponding 2θ values of 30.64°, 35.30°, 46.92°, 54.56° and 74.82° reveal the formation of hexagonal CoS nanoparticles on the p-rGO sheets with average crystallite size of 28 nm based on Scherrer equation using PDXL software [JCPDS card no. 03-065-8977].

The bonding and functional groups present in the CoS-p-rGO nanocomposite were analysed by DRIFT-FTIR spectroscopy. Fig. 2 depicts the characteristic DRIFT spectrum of CoS-p-rGO. The peak at 3729 $cm^{-1}$ corresponds to the stretching of —OH groups. The peaks positioned at 1079 and 1623 $cm^{-1}$ are due to the bending vibration of sulphonated and adsorbed $H_2O$ in the nanocomposite. The peaks at 767 and 618 $cm^{-1}$ are attributed to the stretching vibration of Co-S bonds [29].

The morphology and microstructure of the synthesized CoS nanoparticles on the p-rGO sheets were examined through FESEM and HRTEM analysis. The FESEM images of the synthesized nanocomposite material are displayed in Fig. 3. TEM and HRTEM images of the CoS-p-rGO nanocomposite material are shown in Fig. 4. The FESEM and low resolution TEM images (Figs. 3 and 4 (a and b)) indicate the homogeneous distribution of CoS nanoparticles on the p-rGO sheets. The average CoS particle size of the synthesized nanocomposite was calculated using Image J software and was found to be around 3.16 ± 0.076 nm. TEM images suggests that the CoS particles underwent agglomeration during the synthesis. The HRTEM images of the CoS-p-rGO nanocomposite (Fig. 4c and d) indicate the formation of a crystalline structure. The selected area electron diffraction (SAED) pattern confirms the crystalline structure of the sample by the presence of (100), (101), and (110) crystalline planes (Fig. 4e).

Information about the surface electronic state of the Co and S atoms and the chemical composition of the synthesized nanocomposite were obtained from XPS analysis. The $S_{2p}$ spectrum (Fig. 5) exhibits a band at 161.5 eV, characteristic of CoS, and an additional peak at 167.5 eV due to the presence of partially oxidized sulphur ion. The $Co_{2p}$ spectrum (Fig. 5) displays bands due to CoS at 778.8 and 794.0 eV with a spin-orbit splitting of 15.2 eV as expected for CoS. The bands at 781.7 and 797.6 eV with spin-orbit splitting of 15.9 eV are assigned to $CoSO_4$ with additional satellite peaks due to $Co^{2+}$ at 781.6 and 803.9 eV. The high resolution XPS spectrum of $C_{1s}$ indicates the presence of $sp^2$ hybridized C-atoms (284.3 eV) and thus reduced GO together with bands for C—C/C-S (285.3 eV), C—O (286.2 eV) and C═O (287.7 eV). The overall $Co_{2p}$ and $S_{2p}$ content in CoS-p-rGO are found to be 17.5 and 21.5%, respectively.

The BET specific surface area of the p-GO was found to be 301.476 $m^2/g$ with a pore volume of 0.099 $cm^3/g$ and a pore radius

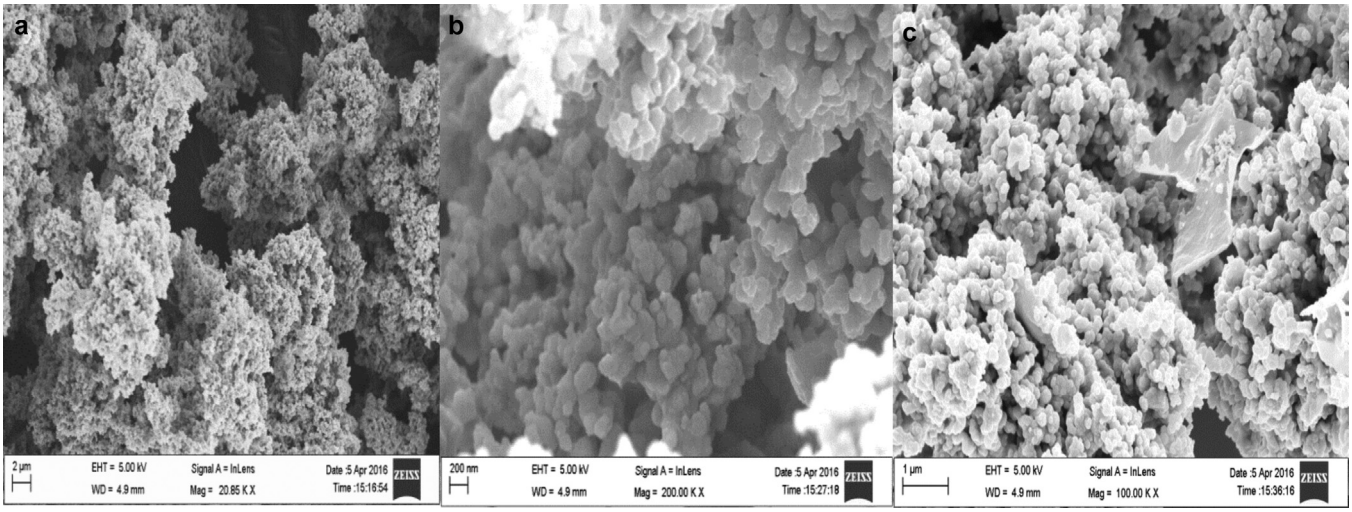


**Fig. 3.** FESEM images of CoS-p-rGO nanocomposite.

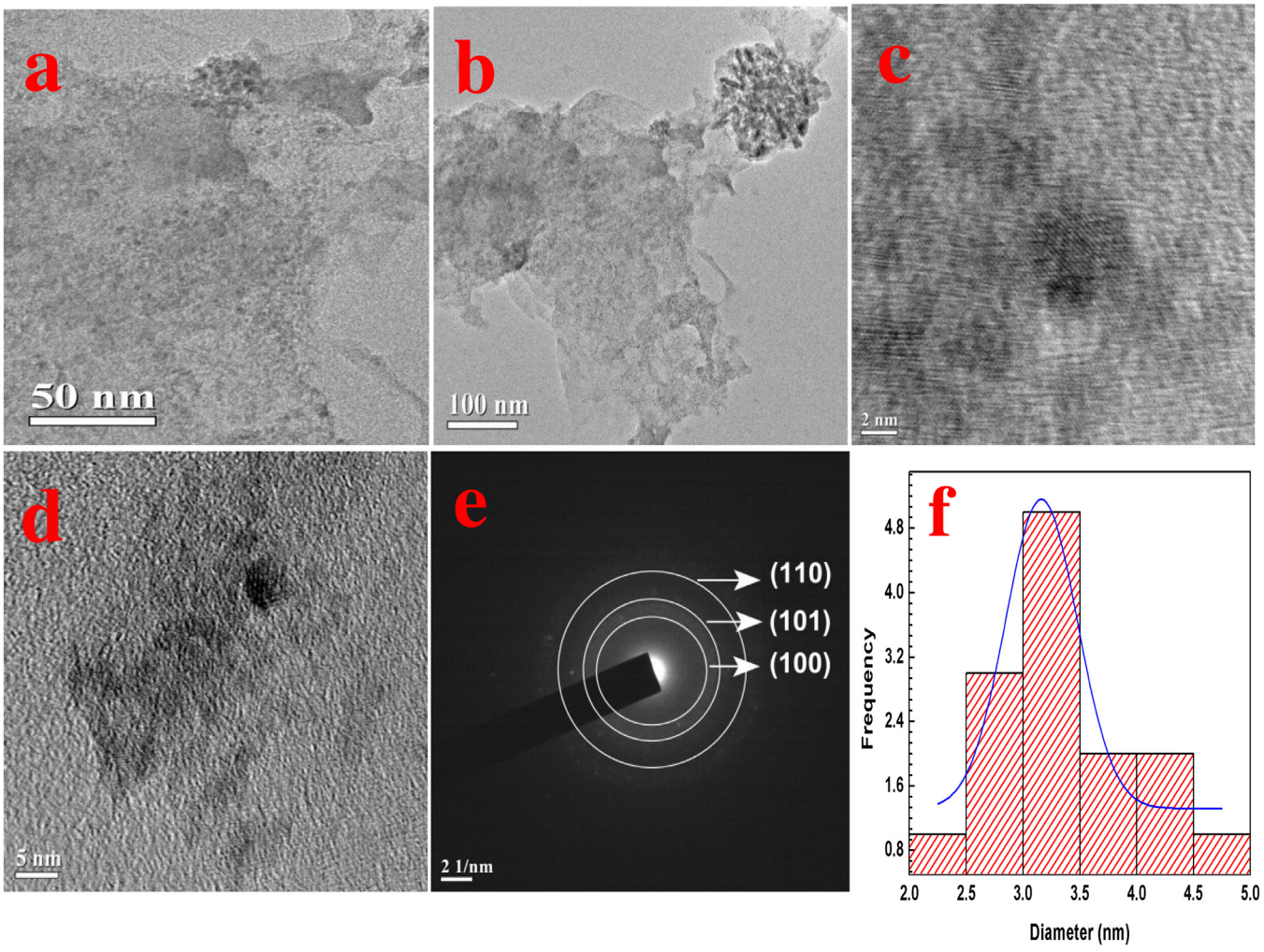


**Fig. 4.** TEM images (a,b), HRTEM images (c,d), SEAD pattern (e) and particle size distribution (f) of CoS-p-rGO nanocomposite.

of 1.88 nm. The surface area value is comparable to that of p-GO reported by Tandiana et al. [28]. On the other hand, after decorating CoS nanoparticles on the p-GO surface, the surface area of the CoS-p-rGO nanocomposite decreased to 56.94 $m^2/g$ with a pore volume 0.126 $cm^3/g$. The average pore radius of CoS-p-rGO remains at 1.79 nm, based on the Barrett-Joyner-Halenda (BJH) plot. The typical $N_2$ adsorption-desorption isotherm with corresponding pore size distribution of CoS-p-rGO are shown in Fig. S3.

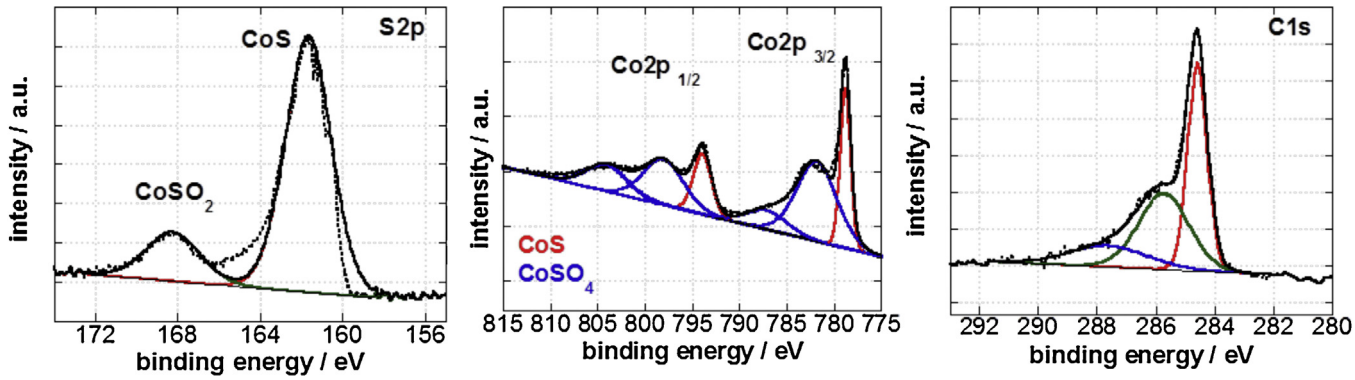


**Fig. 5.** High resolution X-ray photoelectron spectra of CoS-p-rGO nanocomposite: $S_{2p}$, $Co_{2p}$ and $C_{1s}$ regions.

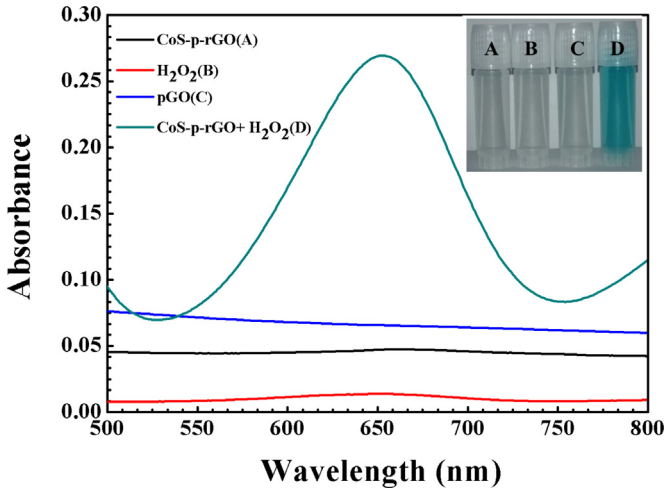


**Fig. 6.** Absorption curves of the reaction products of TMB in the presence of different catalysts in sodium acetate buffer (0.2 M, pH 3, 2.5 mL), 0.5 mM TMB, 50 μL of 30% $H_2O_2$, temperature: 45 °C and 3 mg/L (A) CoS-p-rGO, (B) $H_2O_2$, (C) pGO and (D) CoS-p-rGO + $H_2O_2$.

### 3.2. Peroxidase like activity of CoS-p-rGO nanocomposite

The peroxidase-like catalytic activity of CoS-p-rGO nanocomposite was investigated by analysing the oxidation of TMB in the presence and absence of $H_2O_2$. CoS-p-rGO as well as p-GO alone did not result in the oxidation of TMB in acetate buffer and no colour change was observed. The use of CoS-p-rGO in the presence of $H_2O_2$ turns the solution blue due to the oxidation of TMB to 3,3′,5,5′-tetramethylbenzidine diimine (TMBDI), which has a maximum absorption peak at 652 nm (Fig. 6). The peroxidase-like activity of CoS-p-rGO nanocomposite can be briefly explained through a Fenton reaction mechanism as shown below [26]:

$$Co(II) + H_2O_2 \rightarrow Co(III)OH + {}^{\bullet}OH$$

$$Co(III)OH + H_2O_2 \rightarrow Co(II) + H_2O + HOO^{\bullet}$$

$$TMB + {}^{\bullet}OH \rightarrow \text{ox-TMB (bluecolour)}$$

The catalytic activity of CoS-p-rGO towards TMB oxidation reaction depends on the temperature and pH of the medium. We analysed the peroxidase-like activity of the catalyst in the temperature range from 25 to 55 °C and pH from 2 to 7. Fig. 7a depicts the variation of the catalytic activity of CoS-p-rGO towards TMB oxidation in presence of $H_2O_2$ at different temperatures. Maximal catalytic activity was recorded at 45 °C, pH 3 and a concentration of CoS-p-rGO of 7 mg/L (Fig. 7b, c). Thus, our optimal experimental conditions were pH 3, 45 °C and 7 mg/L of CoS-p-rGO nanocomposite.

**Table 1**
Michaelis-Menten constant ($K_m$) and maximum reaction rate ($V_m$) for CoS-p-rGO, CoS-rGO and CoS nanocomposites.

| Catalysts | Substances | $K_m$ (mM) | $V_m$ ($10^{-8}$ $Ms^{-1}$) |
|---|---|---|---|
| CoS-p-rGO | $H_2O_2$ | 0.1114 | 12.2 |
| CoS-p-rGO | TMB | 0.3380 | 5.0 |
| CoS-rGO | $H_2O_2$ | 0.16 | 2.4 |
| CoS-rGO | TMB | 0.36 | 5.01 |
| CoS | $H_2O_2$ | 0.26 | 0.6127 |
| CoS | TMB | 0.41 | 8.4459 |

### 3.3. Kinetic analysis of CoS-p-rGO as peroxidase mimics and determination of Michaelis constant

Kinetic analysis was studied by changing the concentration of the substrates (TMB and $H_2O_2$), while keeping the concentration of other reagents constant. The value of absorbance at a particular concentration of the substrate was calculated using Beer Lambert's law:

$$A = \epsilon_{TMBDI} \times C \times L$$

where $\epsilon_{TMBDI} = 39{,}000\ M^{-1}cm^{-1}$ at 652 nm and A is the absorbance [30]. C is the concentration of the substrate and L is the path length. Fig. 8 displays the typical Michaelis-Menten curves. The catalytic parameters $K_m$ (Michaelis constant) and $V_m$ (maximal velocity) of the enzyme mimics CoS-p-rGO were evaluated from Lineweaver Burk double reciprocal plots (Fig. 8a and b insets). For comparison, the peroxidase-like catalytic activity of CoS and CoS-rGO nanocomposite was investigated by analysing the oxidation of peroxidase substrate TMB in the presence of $H_2O_2$ under same experimental conditions as for CoS-p-rGO. Similarly, in the presence of CoS and CoS-rGO, the TMB solution exhibited a maximum absorption peak at 652 nm, indicating the formation of oxidized product of TMB by $H_2O_2$. Kinetic analysis was studied by changing the concentration of the substrates (TMB and $H_2O_2$), while keeping the concentration of other reagents constant. Figs. S9 and S10 depict the typical Michaelis-Menten curves for TMB and $H_2O_2$, respectively as substrates in a certain concentration range in presence of CoS and CoS-rGO nanocomposite. The catalytic parameters $K_m$ (Michaelis constant) and $V_m$ (maximal velocity) of the enzyme mimics CoS and CoS-rGO were evaluated from Lineweaver Burk double reciprocal plots (Figs. S9 and S10 insets). The $K_m$ and $V_m$ values for all the three catalysts CoS-p-rGO, CoS-rGO, CoS are listed in Table 1. The low $K_m$ values for the three catalysts suggest significant affinity towards both TMB and $H_2O_2$. The lowest $K_m$ value (0.3380 for TMB) exhibited by CoS-p-rGO indicates its better substrate affinity

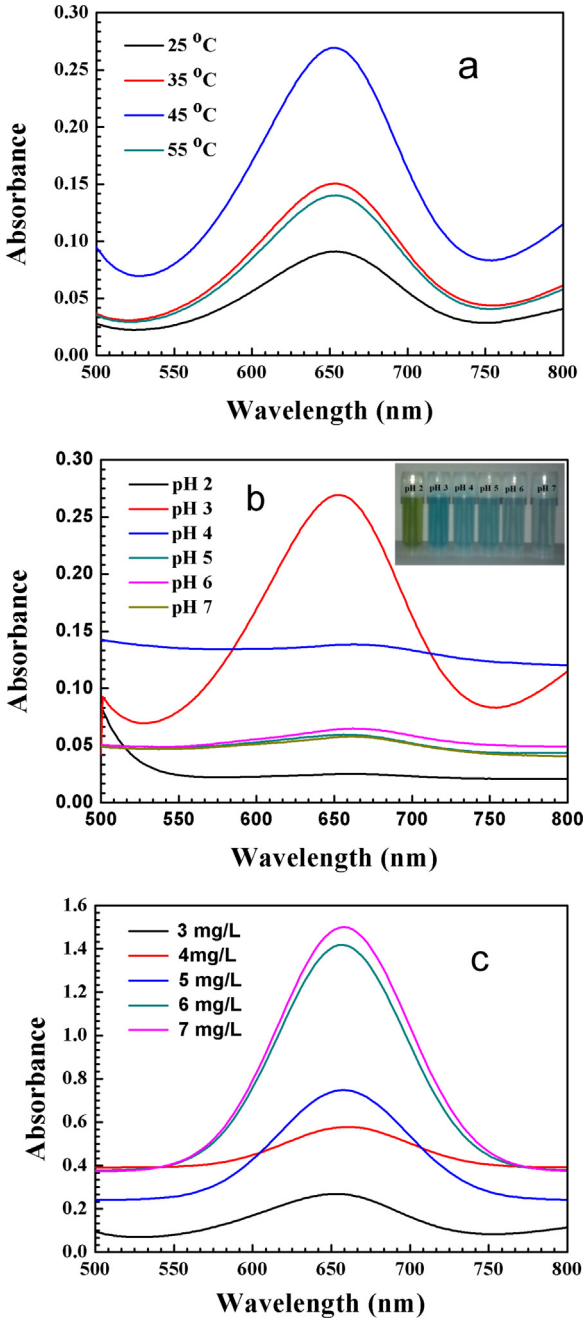


**Fig. 7.** (a) UV–vis absorption spectra of TMB using 3 mg/L CoS-p-rGO at different temperatures in sodium acetate buffer (0.2 M, pH 3, 2.5 mL), 0.5 mM TMB, and 50 μL of 30% $H_2O_2$, pH 3; (b) UV–vis absorption spectra of TMB using 3 mg/L CoS-p-rGO at different pH in sodium acetate buffer (0.2 M, pH 3, 2.5 mL), 0.5 mM TMB, and 50 μL of 30% $H_2O_2$, temperature: 45 °C; (c) UV–vis absorption spectra of TMB using different concentrations of CoS-p-rGO in sodium acetate buffer (0.2 M, pH 3, 2.5 mL), 0.5 mM TMB, and 50 μL of 30% $H_2O_2$, temperature: 45 °C, pH 3.

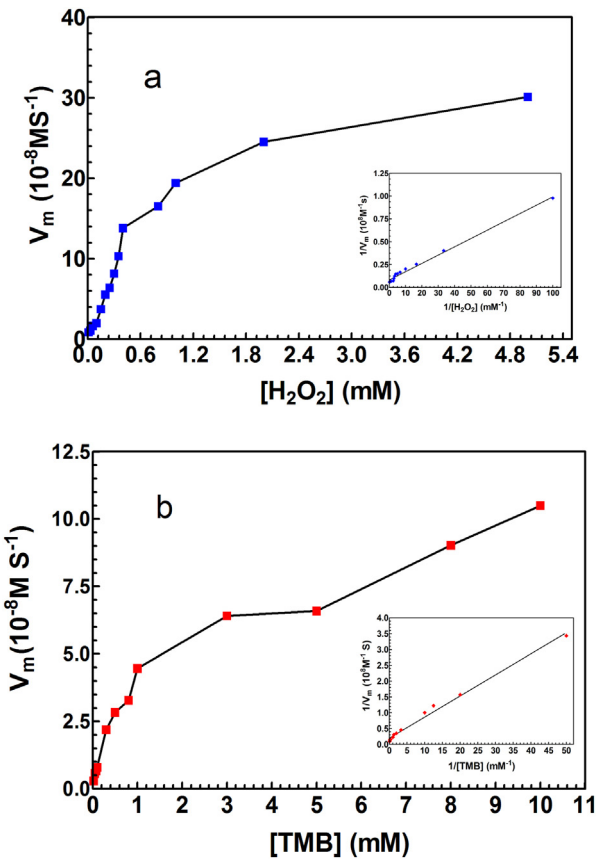


**Fig. 8.** Steady-state kinetic assay and catalytic mechanism of CoS-p-rGO: (a) Variation of $H_2O_2$ concentration (0.01–5.0 mM) at constant TMB concentration (0.5 mM), (b) Variation of TMB concentration (0.02–10.0 mM) at constant $H_2O_2$ concentration (50 mM). The corresponding Lineweaver–Burk plots of the double reciprocal of Michaelis-Menten equation are shown in the insets.

in comparison to CoS-rGO and CoS towards TMB. Also, the $K_m$ value obtained for CoS-p-rGO with $H_2O_2$ is much lower, signifying that lower $H_2O_2$ concentration is required for TMB oxidation than many other enzyme mimics.

### 3.4. Sensitivity of CoS-p-rGO for metal ions detection

The CoS-p-rGO nanocomposite was in addition investigated for the possibility to detect heavy metal ions. From the above experimental results, it was found that CoS-p-rGO catalyses the oxidation of TMB in presence of $H_2O_2$ to form a blue coloured solution having a strong absorption peak at 652 nm. Whenever metal ions like Hg(II), Pb(II) and Cd(II) are added, the catalytic activity of CoS-p-rGO is inhibited. The variation of the UV–vis spectra of the oxidized TMB in the presence and absence of Hg(II) ions is depicted in Fig. 9a. This inhibition is attributed to the strong binding affinities of the metal ions to the S containing sites of the catalyst, which block the active sites of the catalyst surface [22].

To investigate the sensitivity of the nanocomposite materials towards Hg(II) ion, we investigated the UV–vis response upon addition of Hg(II) ion to the TMB+ $H_2O_2$ system by keeping all the other parameters constant (Fig. 9b). In this case, the absorbance decreases with increasing the concentration of metal ions. Fig. 9b (inset) shows that the catalyst displays a linear response towards Hg(II) ions in the concentration range of 2–100 nM ($R^2$ = 0.9813). The limit of detection (LOD) defined as 3.3 σ/slope is determined to be 14.23 nM (Standard deviation (σ) = 0.00931 and slope = 0.002159). It was observed that the LOD was lower in comparison to the maximum contamination level of Hg(II) ion in drinking water (30 nM) permitted by the World Health Organization (WHO) [31]. Table 2 presents a comparative study for the detection of Hg(II) ion adopting different colorimetric probes.

For selectivity, we also investigated the oxidation of TMB + $H_2O_2$ system in presence of 0.5 μM of Pb(II), Cd(II) and Hg(I) ions. No significant change was observed in the absorbance of ox-TMB at the wavelength of 652 nm in the presence of Hg(I) ions, while a small change was observed for Pb(II) and Cd(II), as shown in Fig. 9c. Thus it can be concluded that the synthesized nanocomposite has good selectivity for Hg(II) ion. The selectivity is attributed to the very low $K_{sp}$ value of HgS ($2 \times 10^{-52}$) as comparable to the $K_{sp}$ value of CoS

**Table 2**
Comparison of different methods using different materials for Hg(II) ions detection.

| Materials | Detection Methods | LOD | Linear Range | Ref. |
|---|---|---|---|---|
| Graphene–gold nanocomposite | Colorimetry | 16 nM | 0–3.5 μM | [32] |
| Graphene quantum dots | Fluorescence | 0.12 μM | 0.15–20 μM | [33] |
| BSA–Pt nanozyme | Colorimetry | 7.2 nM | 0–120 nM | [17] |
| Silver nanoparticles | Colorimetry | 2.73 nM | 0–13.6 nM | [34] |
| Graphene oxide-gold nanohybrids | Colorimetry | 300 nM | – | [21] |
| Cu-based MOF | Colorimetry | 0.22 μM | 3–40 μM | [22] |
| CoS-p-rGO | Colorimetry | 14.23 nM | 2–100 nM | Present study |

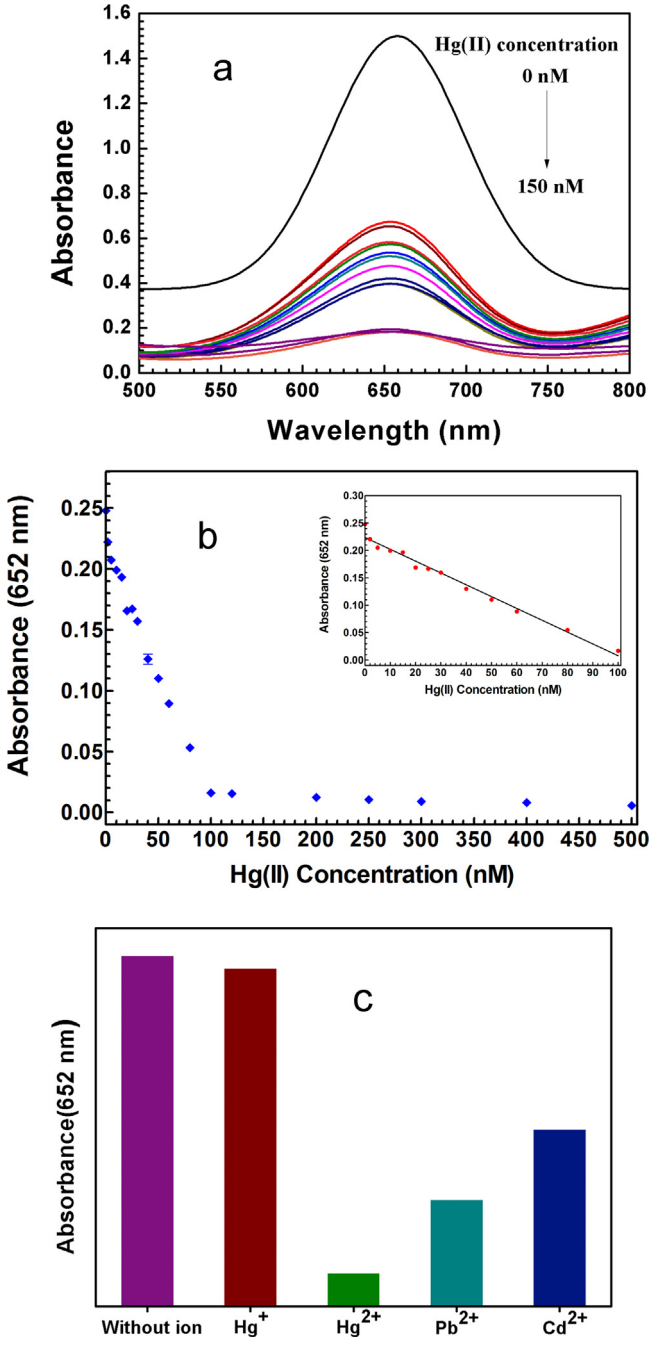


**Fig. 9.** (a) UV–vis spectra of the oxidized TMB product in presence and absence of Hg(II) ion (0.5 mM TMB in acetate buffer (0.2 M, pH 3, 2.5 mL), 7 mg/L CoS-p-rGO, 50 μL $H_2O_2$, temperature: 45 °C; (b) plots of the absorbance values versus Hg(II) concentration, inset: standard linear calibration plots of the reaction system at different concentrations of Hg(II); (c) Absorbance of the ox-TMB in presence of 0.5 μM of different ions (0.5 mM TMB, acetate buffer (0.2 M, pH 3, 2.5 mL), 7 mg/L CoS-p-rGO and 50 μL $H_2O_2$, temperature: 45 °C).

$(4 \times 10^{-21})$, PbS $(3 \times 10^{-28})$ and CdS $(8 \times 10^{-28})$. Therefore, HgS is formed at the interface of the active binding sites of the catalyst surface and inhibits the catalytic efficiency of the catalyst towards peroxidase oxidation of TMB.

The effect of time on the peroxidase activity of CoS-p-rGO catalyst in presence of 0.05 μM Hg(II) ions was investigated by keeping the reaction mixture for 3 h under same experimental conditions and the absorbance of the oxidized TMB product was recorded at different time intervals at wavelength 652 nm (Fig. S11). It was found that by increasing the contact time more Hg(II) ions are bound to the catalyst surface and thus more active sites are occupied by the ions, inhibiting its catalytic efficiency towards peroxidase oxidation of TMB. Therefore, the blue colour of the oxidized product has turned into green colour with increasing the contact time.

To study the effect of co-existing different natural organic matters (NOM) like chlorophyll, humic acid and phenol with Hg(II) ions in aqueous system on the variation of the absorbance of blue coloured ox-TMB solution, the peroxidase oxidation of TMB in presence of CoS-p-rGO was carried out under the same experimental conditions in presence of 1 mg/L of each NOM with 0.05 μM Hg(II) ions separately. It was found that in presence of chlorophyll and phenol, the blue colour of the solution of ox-TMB turns green and the absorbance of ox-TMB solution is lower than that of the solution containing only Hg(II) ions, suggesting that more Hg(II) ions are bound with the catalyst surface in presence of these species which lowers the peroxidase efficiency of the catalyst. Whereas in presence of humic acid the absorbance of the ox-TMB solution is higher than that of the solution containing Hg(II) ions alone. Humic acid inhibits the binding of Hg(II) ions with the catalyst surface and blocks the active sites present on the catalyst. Therefore, the peroxidase activity of the catalyst is increased as compared to the solution containing Hg(II) alone. The variation of UV–vis spectral changes in presence of different NOM with Hg(II) ions is shown in Fig. S12.

### 3.5. Detection of Hg(II) ion in environmental samples

The practical sensor application of the synthesized materials was investigated for the detection of Hg(II) ion in different environmental samples. The percentage recovery and relative standard deviation in different environmental samples are displayed in Table 3 (n = 3). The proposed method showed good recovery percentage for Hg(II) ions in different environmental samples. The results suggest that the proposed sensor can be effectively used for the detection of Hg(II) ions in real samples with good recovery values.

## 4. Conclusion

In summary, we have successfully synthesized CoS nanoparticles on porous reduced graphene oxide sheets by a simple solvothermal method and successfully used as a peroxidase mimic system for the detection of Hg(II) ion colorimetrically. The synthesized nanocomposite showed highly efficient peroxidase-like activity for the oxidation of peroxidase substrate TMB into blue

**Table 3**
Recovery of Hg(II) ions in environmental samples.

| Samples | Hg(II) added (nM) | Hg(II) found (nM) | Recovery[n] (%) | RSD[n] (%) |
|---|---|---|---|---|
| Tap water | 10 | 9.93 | 99.30 | 0.46 |
| | 30 | 29.50 | 98.33 | 1.50 |
| | 100 | 99.94 | 99.94 | 0.05 |
| Tube well water | 10 | 9.85 | 98.50 | 0.36 |
| | 30 | 28.68 | 95.59 | 1.70 |
| | 100 | 99.41 | 99.41 | 0.33 |
| Pond water | 10 | 9.91 | 99.10 | 0.46 |
| | 30 | 29.34 | 97.81 | 0.87 |
| | 100 | 98.52 | 98.52 | 0.08 |
| Brahmaputra river water | 10 | 9.87 | 98.70 | 0.51 |
| | 30 | 29.92 | 99.72 | 0.13 |
| | 100 | 99.49 | 99.49 | 0.44 |

coloured oxidized TMB. Moreover, the presence of porous reduced graphene oxide nanosheets provided high surface area for CoS particles hence CoS-p-rGO nanocomposite exhibited better catalytic efficiency in comparison to CoS and CoS-rGO nanocomposite materials with a detection limit of 14.23 nM for Hg(II) ions. The strong interaction between metal ions like Hg(II) and −S atoms of the nanocomposite played a significant role in the qualitative and quantitative determination of Hg(II) ions. Thus this simple, cost effective and easy colorimetric technique using metal sulphide nanocomposite materials has potential applications in toxic Hg(II) ion detection in various environmental samples.

## Acknowledgements

The authors are grateful to the Director, CSIR-NEIST, Jorhat for his interest to carry out the work. PB and GD acknowledge DST, New Delhi, India for DST-INSPIRE Fellowship grant. We also acknowledge the CSIR-NEIST, Jorhat (CSC-0408) for the FESEM facility and SAIF, NEHU, Shillong for HRTEM facility.

## Appendix A. Supplementary data

Supplementary data associated with this article can be found, in the online version, at http://dx.doi.org/10.1016/j.snb.2016.12.148.

## References

[1] I. Sierra, D. Perez-Quintanilla, Heavy metal complexation on hybrid mesoporous silicas: an approach to analytical applications, Chem. Soc. Rev. 42 (2013) 3792–3807.
[2] X. Zhou, J. Nie, B. Du, 4-(2-Pyridylazo)-resorcinol functionalized thermosensitive ionic microgels for optical detection of heavy metal ions at nanomolar level, ACS Appl, Mater. Interfaces 7 (2015) 21966–21974.
[3] T.W. Clarkson, L. Magos, G.J. Myers, The toxicology of mercury–current exposures and clinical manifestations, N. Engl. J. Med. 349 (2003) 1731–1737.
[4] R.K. Zalups, Molecular interactions with mercury in the kidney, Pharmacol. Rev. 52 (2000) 113–143.
[5] I. Hoyle, R.D. Handy, Dose-dependent inorganic mercury absorption by isolated perfused intestine of rainbow trout, Oncorhynchus mykiss, involves both amiloride-sensitive and energy-dependent pathways, Aquat. Toxicol. 72 (2005) 147–159.
[6] H.L. Needleman, D. Bellinger, The health effects of low level exposure to lead, Annu. Rev. Public Health 12 (1991) 111–140.
[7] D.M. Templeton, Y. Liu, Multiple roles of cadmium in cell death and survival, Chem. Biol. Interact. 188 (2010) 267–275.
[8] A. Malekpour, S. Hajialigol, M.A. Taher, Study on solid-phase extraction and flame atomic absorption spectrometry for the selective determination of cadmium in water and plant samples with modified clinoptilolite, J. Hazard. Mater. 172 (2009) 229–233.
[9] S. Yunus, S. Charles, F. Dubois, E.V. Donckt, Simultaneous determination of cadmium(II) and zinc(II) by molecular fluorescence spectroscopy and multiple linear regression using an anthrylpentaazamacrocycle chemosensor, J. Fluoresc. 18 (2008) 499–506.
[10] A.M. Bond, G.G. Wallace, Simultaneous determination of copper, nickel, cobalt, chromium(VI), and chromium(III) by liquid chromatography with electrochemical detection, Anal. Chem. 54 (1982) 1706–1712.
[11] D. Beauchemin, S.S. Berman, Determination of trace metals in reference water standards by inductively coupled plasma mass spectrometry with on-line preconcentration, Anal. Chem. 61 (1989) 1857–1862.
[12] W. Guo, S. Hu, Y. Xiao, H. Zhang, X. Xie, Direct determination of trace cadmium in environmental samples by dynamic reaction cell inductively coupled plasma mass spectrometry, Chemosphere 81 (2010) 1463–1468.
[13] F. Seby, S. Charles, M. Gagean, H. Garraud, O.F.X. Donard, Chromium speciation by hyphenation of high-performance liquid chromatography to inductively coupled plasma-mass spectrometry – study of the influence of interfering ions, J. Anal. At. Spectrom. 18 (2003) 1386–1390.
[14] D. Lin, J. Wu, M. Wang, F. Yan, H. Ju, Triple signal amplification of graphene film, polybead carried gold nanoparticles as tracing tag and silver deposition for ultrasensitive electrochemical immunosensing, Anal. Chem. 84 (2012) 3662–3668.
[15] N. Bi, Y. Chen, H. Qi, X. Zheng, Y. Chen, X. Liao, et al., A sensitive localized surface plasmon resonance sensor for determining mercury(II) ion using noble metal nanoparticles as probe, Spectrochim. Acta Part A 95 (2012) 276–281.
[16] L. Tan, Y. Zhang, H. Qiang, Y. Li, J. Sun, L. Hu, Z. Chen, A sensitive Hg(II) colorimetric sensor based on synergistic catalytic effect of gold nanoparticles and Hg, Sens. Actuators B 229 (2016) 686–691.
[17] W. Li, B. Chen, H. Zhang, Y. Sun, J. Wang, J. Zhang, Y. Fu, BSA-stabilized Pt nanozyme for peroxidase mimetics and its application on colorimetric detection of mercury(II) ions, Biosens. Bioelectron. 66 (2015) 251–258.
[18] D. Zhang, Z. Chen, H. Omar, L. Deng, N.M. Khashab, Colorimetric peroxidase mimetic assay for uranyl detection in sea water, ACS Appl. Mater. Interfaces 7 (2015) 4589–4594.
[19] G.W. Wu, S.B. He, H.P. Peng, H.H. Deng, A.L. Liu, X.H. Lin, X.H. Xia, W. Chen, Citrate-capped platinum nanoparticle as a smart probe for ultrasensitive mercury sensing, Anal. Chem. 86 (2014) 10955–10960.
[20] Z.q. Tan, J.f. Liu, Visual test of subparts per billion-level mercuric ion with a gold nanoparticle probe after preconcentration by hollow fiber supported liquid membrane, Anal. Chem. 82 (2010) 4222–4228.
[21] X. Chen, N. Zhai, J.H. Snyder, Q. Chen, P. Liu, L. Jin, et al., Colorimetric detection of Hg2+ and Pb2+ based on peroxidase-like activity of graphene oxide-gold nanohybrids, Anal. Methods 7 (2015) 1951–1957.
[22] Y. Xiong, L. Su, H. Yang, P. Zhang, F. Ye, Fabrication of copper sulfide using a Cu-based metal organic framework for the colorimetric determination and the efficient removal of Hg2+ in aqueous solutions, New J. Chem. 39 (2015) 9221–9227.
[23] G. Nie, L. Zhang, X. Lu, X. Bian, W. Sun, C. Wang, A one-pot and in situ synthesis of CuS-graphene nanosheet composites with enhanced peroxidase-like catalytic activity, Dalton Trans. 42 (2013) 14006–14013.
[24] S. Dutta, C. Ray, S. Mallick, S. Sarkar, R. Sahoo, Y. Negishi, T. Pal, A gel-based approach to design hierarchical CuS decorated reduced graphene oxide nanosheets for enhanced peroxidase-like activity leading to colorimetric detection of dopamine, J. Phys. Chem. C 119 (2015) 23790–23800.
[25] J. Peng, J. Weng, Enhanced peroxidase-like activity of $MoS_2$/graphene oxide hybrid with light irradiation for glucose detection, Biosens. Bioelectron. 89 (2017) 652–658.
[26] E. Spier, U. Neuenschwander, I. Hermans, Insights in the Cobalt(II)-catalyzed decomposition of peroxide, Angew. Chem. Int. Ed. 52 (2013) 1581–1585.
[27] W.S. Hummers Jr., R.E. Offeman, Preparation of graphitic oxide, J. Am. Chem. Soc. 80 (1958) 1339.
[28] C. Su, R. Tandiana, J. Balapanuru, W. Tang, K. Pareek, C.T. Nai, et al., Tandem catalysis of amines using porous graphene oxide, J. Am. Chem. Soc. 137 (2015) 685–690.
[29] S. Ariponnammal, T. Srinivasan, Growth and characterization of cobalt sulphide nanorods, Res. J. Recent. Sci. 2 (2013) 102–105.
[30] A.K. Dutta, S.K. Maji, D.N. Srivastava, A. Mondal, P. Biswas, P. Paul, B. Adhikary, Synthesis of FeS and FeSe nanoparticles from a single source precursor: A study of their photocatalytic activity, peroxidase-like behavior, and electrochemical sensing of H2O2, ACS Appl. Mater. Interfaces 4 (2012) 1919–1927.
[31] N. Pirrone, K.R. Mahaffey, Dynamics of Mercury Pollution on Regional and Global Scales: Atmospheric Processes and Human Exposures Around the World, 2005.
[32] Z. Yan, H. Xue, K. Berning, Y.W. Lam, C.S. Lee, Identification of multifunctional graphene-gold nanocomposite for environment-friendly enriching separating, and detecting Hg2+ simultaneously, ACS Appl. Mater. Interfaces 6 (2014) 22761–22768.
[34] Y. Bhattacharjee, A. Chakraborty, Label-free cysteamine-capped silver nanoparticle-based colorimetric assay for Hg(II) detection in water with subnanomolar exactitude, ACS Sus. Chem. Eng. 2 (2014) 2149–2154.

## Biographies

**Priyakshree Borthakur** received her M.Sc. degree in Chemistry from Dibrugarh University, Dibrugarh, Assam, India in 2013. She is currently a research student in the Advanced Materials Group, Materials Sciences and Technology Division of CSIR-North East Institute of Science and Technology, Jorhat, India. Her research interests

include decoration of metal sulphide nanoparticles on different two dimensional materials and their applications in various fields like photocatalysis, sensor etc.

**Gitashree Darabdhara** GD received her M.Sc degree in Chemistry in 2013 from Gauhati University, Guwahati, Assam, India. She is currently a research student in the Advanced Materials Group, Material Sciences and Technology Division of CSIR-North East Institute of Science and Technology, Jorhat, India. Her research interest is in the field of synthesis of different bimetallic nanoparticles on graphene oxide nanosheets and their application in various fields like photocatalysis, biosensing, hydrogen evolution reactions, organic catalytic transformations etc.

**Manash R. Das** is a Research Scientist at Materials Sciences and Technology Division, CSIR-North East Institute of Science and Technology (CSIR-NEIST), Jorhat, India since 2008. He is also an Assistant Professor in Academy Council of Scientific and Innovative Research (AcSIR), India. Dr Das received his PhD degree from Dibrugarh University, Assam, India in 2007 in the field of Surface Chemistry. He worked as a postdoctoral fellow with Dr. Rabah Boukherroub at the Interdisciplinary Research Institute (IRI), France during 2007 and 2008. He has published more than 60 peer reviewed research articles and eight book chapters. His research interests include graphene and other 2D materials decoration with metal nanoparticles, bimetallic nanoparticles and metal oxide and their applications in organic catalysis reaction, photocatalysis, water pollutant removal, sensor.

**Rabah Boukherroub** is a research director at the CNRS and a group leader at the Institute of Electronics, Microelectronics and Nanotechnology, University Lille1, France. He is Associate Editor for ACS Applied Materials & Interfaces. His research interests are in the area of synthesis of functional nanomaterials, surface chemistry, and photophysics of semiconductor/metal nanostructures with emphasis on biosensors, drug delivery, and photocatalysis. He is a co-author of more than 400+ research publications and wrote 29 book chapters in subjects related to nanotechnology, materials chemistry, and biosensors. He has 9 patents or patents pending.

**Sabine Szunerits** is since 2009 Professor in Chemistry at the University Lille 1, France and was nominated in 2011 as a member of the "Institut Universitaire de France" (IUF). Her current research interests are in the area of materials science with emphasis on the development of novel analytical platforms and interfaces for the study of affinity binding events and in the modification of nanostructures (diamond particles, magnetic particles, nanographene) for biomedical applications. She is co-author of more than 240 research publications, wrote several book chapters and has 6 patents.